Bulletin of the Seismological Society of America, Vol. 93, No. 6, pp. 2531–2545, December 2003

Source Characterization for Broadband Ground-Motion Simulation: Kinematic Heterogeneous Source Model and Strong Motion Generation Area

by Hiroe Miyake, Tomotaka Iwata, and Kojiro Irikura

Abstract We estimate strong motion generation areas that reproduce near-source ground motions in a broadband frequency range (0.2–10 Hz) using the empirical Green's function technique. The strong motion generation areas are defined as extended areas with relatively large slip velocities within a total rupture area. Four M 6 class (the 1997 Kagoshima on March and May, 1997 Yamaguchi, and 1998 Iwate) and several moderate-size earthquakes in Japan were analyzed. We examine the relationship between the strong motion generation area and the area of asperities, which is characterized based on heterogeneous slip distributions estimated from low-frequency ($<$1 Hz) waveform inversions (Somerville *et al.*, 1999). We performed waveform fitting in acceleration, velocity, and displacement, then obtained the strong motion generation area occupying about a quarter of the total rupture area. The size and position of the strong motion generation area coincide with those of characterized asperities. We find self-similar scaling of seismic moment to both the size of the strong motion generation area and the rise time for a magnitude range of analyzed earthquakes. Based on our results, we propose a characterized source model for the broadband ground-motion simulation, which consists of strong motion generation areas with large slip velocities and a background slip area with a small slip velocity. Waveform modeling of the characterized source model suggests that the strong motion generation areas play important roles in simulating broadband ground motions and have the potential to be an about 10-MPa stress-release area on the fault.

Introduction

Estimation of spatiotemporal slip distributions for large earthquakes has provided essential information for understanding source physics and rupture mechanisms. Waveform inversions of near-source ground-motion records are expected to have higher resolution than teleseismic waveform inversions, because the former can treat shorter wavelengths. Kinematic waveform inversions based on strong motion records have been carried out since the 1979 Imperial Valley earthquake (e.g., Hartzell and Heaton, 1983). These waveform inversions require good spatial coverage of the source area with observed records and detailed knowledge of the subsurface structures to accurately calculate the theoretical Green's function. Meanwhile, slip distributions of many large crustal earthquakes have been estimated, following the deployment of dense strong motion networks and increased computational power (e.g., the 1989 Loma Prieta by Beroza [1991] and Wald *et al.* [1991]; 1992 Landers by Cohee and Beroza [1994], Wald and Heaon [1994], and Cotton and Compillo [1995]; 1994 Northridge by Wald *et al.* [1996]; 1995 Hyogo-ken Nanbu [Kobe], Japan, by Horikawa *et al.* [1996], Ide *et al.* [1996], Sekiguchi *et al.* [1996, 2000], Wald [1996], and Yoshida *et al.* [1996]; 1999 Kocaeli, Turkey, by Bouchon *et al.* [2002], Delouis *et al.* [2002], and Sekiguchi and Iwata [2002]; and 1999 Chi-Chi, Taiwan, by Chi *et al.* [2001], Ma *et al.* [2001], Wu *et al.* [2001], and Zeng and Chen [2001]). The resolution of waveform inversions is affected by the limit of the usable frequency range when calculating realistic theoretical Green's functions. This limitation is determined by the accuracy of the subsurface structure, which can be validated by waveform modeling of small earthquakes. At present, waveform inversions have been performed successfully up to about 1 Hz for near-source ground-motion velocities. We call such source models, estimated from ground-motion data with frequencies less than 1 Hz, low-frequency source models.

When studying high-frequency (e.g., $>$2 Hz) radiation processes on the fault plane, the problem arises because of the difficulties of calculating the Green's functions deterministically by means of a lack of underground structure information. To overcome this, Zeng *et al.* (1993) and Kak-

ehi and Irikura (1996) proposed an envelope inversion by fitting the envelopes of observed strong motion records to synthetic ones calculated by ray theory in displacement and the empirical Green's function method in acceleration, respectively. Nakahara *et al.* (1998) estimated absolute values of energy intensity by fitting the synthetic acceleration envelopes to observed ones by means of scattering theory. We call these source models high-frequency source models.

In general, slip heterogeneities have been found for most large earthquakes from waveform inversions based on low-frequency (<1 Hz) ground-motion data. Areas of high-frequency (>2 Hz) radiation obtained by envelope inversions largely correspond to regions surrounding the large slip area, branching portions of the fault plane, the area of rupture termination, or the area close to the surface. Both the low- and high-frequency source models can be used to interpret the frequency-dependent mechanisms of strong ground motion generation.

Green's functions for low-frequency ground motions are calculated by a deterministic approach based on coherent summation of rays or wavenumbers. For high-frequency ground motions, Green's functions are calculated by a statistical approach based on random summation. It is therefore difficult to reproduce appropriate Green's functions that satisfy both the amplitude and phase information in the frequency range of 0.5–2.0 Hz, which is very important for earthquake engineering applications (e.g., Kawase, 1998). Note also that the source processes generating 0.5- to 2.0-Hz ground motions are not adequately resolved from either the low- or high-frequency source models. Our objective is to fill the gaps of the source processes shown in the frequency range of 0.5–2.0 Hz.

Source modeling by the empirical Green's function method (e.g., Irikura, 1986; Irikura and Kamae, 1994) is capable of characterizing near-source strong ground motions in a broadband frequency range up to 10 Hz and including 1 Hz. This technique requires observed records from appropriate small events as empirical Green's functions within a broadband frequency range, and the source model is assumed to have a homogeneous slip and rise time with radial rupture propagation from the rupture starting point. High-quality simulations of strong ground motions over a wide frequency range have supported the approval of using an extended area for strong motion generation with this choice of simple parameters (e.g., Kamae and Irikura, 1998a; Miyake *et al.*, 1999, 2001). However, the assumption of homogeneous slip contrasts with the fact that most waveform inversions give heterogeneous slip distributions. Furthermore the areas for strong motion generation are generally smaller than the total rupture areas from waveform inversions. Therefore it is important to clarify the relationship between the source parameters estimated by strong ground motion simulations based on the empirical Green's function method and heterogeneous slip distributions obtained by waveform or envelope inversions.

In this article, we estimate an area we call the strong motion generation area from waveform fitting using the empirical Green's function method in the frequency range of 0.2–10 Hz. The area is defined as extended areas with relatively large slip velocities within a total rupture area. We estimate the size and location of the strong motion generation area and rise time there without any information of low-frequency waveform inversions, then compare the strong motion generation area and asperities identified from waveform inversions. We also examine the scaling of the size of the strong motion generation area and rise time with the seismic moment. For the broadband ground-motion simulation, we propose a characterized source model and calculate the stress drop for the strong motion generation area, taking into consideration the difference between the asperity and crack models (e.g., Das and Kostrov, 1986; Boatwright, 1988).

Data

We investigate the source models of 12 crustal earthquakes (M_w 4.8–6.0) that occurred in Japan from 1996 to 1999 (Table 1; Fig. 1) using near-source ground-motion records. Since the 1995 Hyogo-ken Nanbu (Kobe) earthquake, dense strong motion networks such as the K-NET (Kinoshita, 1998) have been installed across Japan, and they have been consistently recording intermediate-size to large earthquakes on identical instruments and providing good spatial coverage around the source area. We therefore estimated source models of mainshocks by using records of small events as empirical Green's functions, where the events had similar focal mechanisms and hypocenter distances to their respective mainshocks.

Figure 2 shows the epicenters of the mainshocks and their aftershocks, along with the K-NET stations. We use data at stations located within 50 km of the epicenters. The hypocenter locations are obtained from the Faculty of Science, Kyushu University (1997), Faculty of Science, Kagoshima University (1997), and Japan Meteorological Agency (JMA). The focal depths of most earthquakes were less than 20 km. Fault-plane solutions derived by moment tensor inversions (Harvard centroid moment tensor [CMT] catalog by Dziewonski *et al.* [1996, 1997]; Kuge *et al.* [1997, 2003]; National Research Institute for Earth Science and Disaster Prevention (NIED) seismic moment tensor catalog by Fukuyama *et al.* [2000a,b, 2001]), and aftershock distributions (Fukuoka District Meteorological Observatory, JMA, 1998; Miyamachi *et al.*, 1999; Graduate School of Science, Tohoku University, 1999; Umino *et al.*, 1998) were used for determining the orientation of the mainshock fault plane. The waveform fitting for earthquake number 12m was examined for both conjugate fault planes of the moment tensor solution, because the number of aftershock was quite small and the aftershock distribution did not clearly show the fault plane.

Table 1
List of Earthquakes Studied

No.	Date (JST)	Latitude (deg)	Longitude (deg)	Depth (km)	M_{JMA}	M_w (M_0 [N m])	Name of Earthquake
1m	1996/08/11 03:12	38.905N	140.637E	8.63	5.9	5.9 (9.51E + 17)‡	1996 Akita-ken Nairiku Nanbu
1a	1996/08/11 05:39	38.884N	140.651E	9.36	4.2		
2m	1996/08/11 08:10	38.863N	140.676E	9.77	5.7	5.7 (3.84E + 17)‡	1996 Miyagi-ken Hokubu
2a	1996/08/11 15:01	38.849N	140.689E	9.84	4.4		
3m	1997/03/26 17:31	31.970N*	130.380E*	8.2*	6.5	6.0 (1.38E + 18)§	1997 Kagoshima-ken Hokuseibu (March)
3a	1997/03/26 17:39	31.968N*	130.362E*	11.1*	4.7		
4m	1997/05/13 14:38	31.952N†	130.343E†	7.7†	6.3	5.9 (8.89E + 17)§	1997 Kagoshima-ken Hokuseibu (May)
4a	1997/05/25 06:10	31.932N†	130.348E†	(7.7)	4.2		
5m	1997/06/25 18:50	34.438N	131.669E	8.29	6.3	5.8 (5.66E + 17)‖	1997 Yamaguchi-ken Hokubu
5a	1997/06/25 18:58	34.459N	131.696E	13.31	4.0		
6m	1997/09/04 05:15	35.259N	133.379E	8.91	5.1	5.2 (6.83E + 16)‖	1997 Tottori-ken Seibu
6a	1997/09/02 02:07	35.250N	133.381E	13.04	4.1		
7m	1998/02/21 09:55	37.288N	138.771E	20.83	5.0	5.0 (3.15E + 16)‖	1998 Niigata-ken Chubu
7a	1998/02/22 02:49	37.296N	138.775E	22.05	3.7		
8m	1998/04/22 20:32	35.165N	136.570E	10.47	5.4	5.2 (6.74E + 16)‖	1998 Shiga-Gifu Kenkyo
8a	1998/04/22 20:28	35.162N	136.570E	11.21	4.0		
9m	1998/09/03 16:58	39.796N	140.910E	9.63	6.1	5.9 (7.53E + 17)‖	1998 Iwate-ken Nairiku Hokubu
9a	1998/09/03 17:10	39.745N	140.900E	9.86	3.9		
10m	1998/09/15 16:24	38.278N	140.766E	13.25	5.0	5.0 (3.19E + 16)‖	1998 Miyagi-ken Nanbu
10a	1998/09/15 16:18	38.275N	140.766E	12.99	3.6		
11m	1999/02/26 14:18	39.150N	139.850E	19.00	5.1	5.2 (7.19E + 16)‖	1999 Akita-ken Engan Nanbu
11a	1999/03/08 17:46	39.150N	139.850E	21.00	4.2		
12m	1999/03/16 16:43	35.270N	135.935E	12.00	4.9	4.8 (1.83E + 16)‖	1999 Shiga-ken Hokubu
12a	1999/03/22 05:05	35.257N	135.930E	12.40	3.3		

*Hypocenter information from Faculty of Science, Kyushu University (1997).
†Hypocenter information from Faculty of Science, Kagoshima University (1997).
‡Seismic moment determined by Dziewonski *et al.* (1996, 1997) as Harvard CMT catalog.
§Seismic moment determined by Kuge *et al.* (1997).
‖Seismic moment determined by Fukuyama *et al.* (2000a,b, 2001) as NIED seismic moment tensor catalog.
Hypocenter information is provided by the Japan Meteorological Agency unless indicated. The characters "m" and "a" in the first column indicate mainshock and aftershock, respectively. Instead of aftershocks, foreshocks are used as empirical Green's functions for events 6a, 8a, and 10a.

Strong Ground Motion Simulation based on the Empirical Green's Function Method

Formulation of the Empirical Green's Function Method

As stated previously, we define the strong motion generation area as the area characterized by a large uniform slip velocity within the total rupture area, which reproduces near-source strong ground motions up to 10 Hz. The strong motion generation area of each mainshock is estimated by waveform fitting based on the empirical Green's function method. The low-frequency limit is constrained by the signal-to-noise level ratio of the small event record used as an empirical Green's function.

The technique by which waveforms for large events are synthesized follows the empirical Green's function method proposed by Hartzell (1978). Revisions have been made by Kanamori (1979), Irikura (1983, 1986), and others. We use the empirical Green's function method formulated by Irikura (1986), based on a scaling law of fault parameters for large and small events (Kanamori and Anderson, 1975) and the omega-squared source spectra (Aki, 1967). The waveform for a large event is synthesized by summing the records of small events with corrections for the difference in the slip velocity time function between the large and small events following the scaling laws mentioned earlier. This method does not require knowledge of the explicit shape of the slip velocity time function for the small event.

The numerical equations to sum records of small events are

$$U(t) = \sum_{i=1}^{N}\sum_{j=1}^{N} \frac{r}{r_{ij}} F(t)^* (C \cdot u(t)) \quad (1)$$

$$F(t) = \delta(t - t_{ij}) + \frac{1}{n'} \sum_{k=1}^{(N-1)n'} \left[\delta\left\{t - t_{ij} - \frac{(k-1)T}{(N-1)n'}\right\}\right] \quad (2)$$

$$t_{ij} = \frac{r_{ij} - r_o}{V_s} + \frac{\xi_{ij}}{V_r}, \quad (3)$$

where $U(t)$ is the simulated waveform for the large event, $u(t)$ is the observed waveform for the small event, N and C

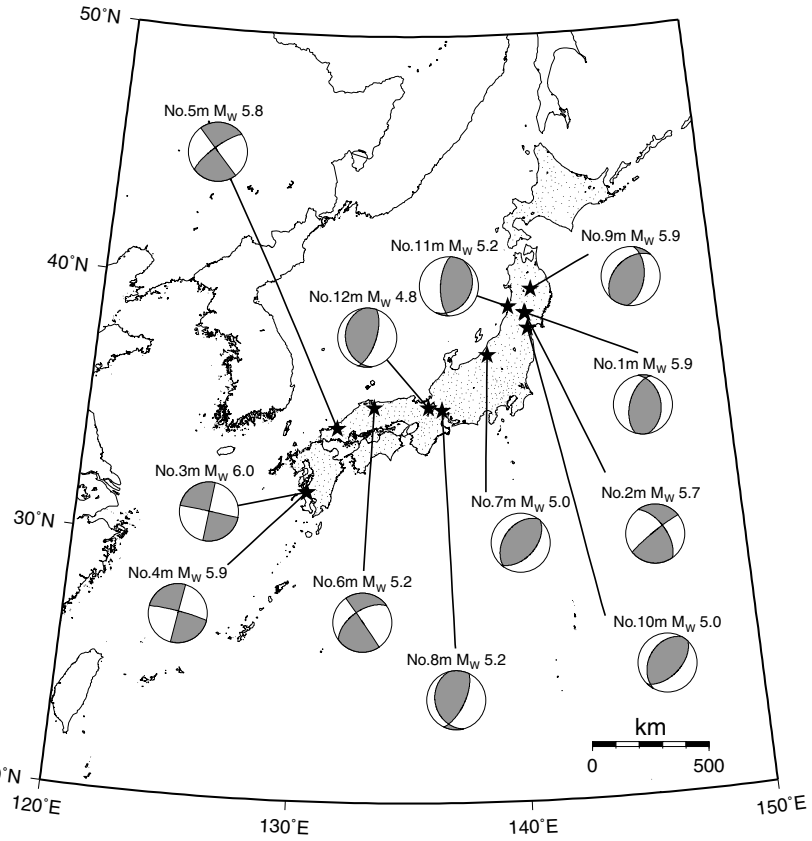

Figure 1. Epicenter locations (solid stars) and focal mechanisms used. Focal mechanisms were determined by moment tensor inversions of broadband seismic waveforms. Black dots indicate the stations of K-NET.

are the ratios of the fault dimensions and stress drops between the large and small events, respectively, and the asterisk indicates convolution. $F(t)$ is the filtering function (correction function) to adjust the difference in the slip velocity time functions between the large and small events. V_s and V_r are the S-wave velocity near the source area and the rupture velocity on the fault plane, respectively. T is the rise time for the large event, defined as the duration of the filtering function $F(t)$ (in Fig. 3b,c). It corresponds the duration of the slip velocity time function on the subfault from the beginning to the time before the tail starts. The variable n' is an appropriate integer to weaken the artificial periodicity of n and to adjust the interval of the tick to be the sampling rate. The other parameters are given in Figure 3a.

Regarding the filtering function $F(t)$, Irikura *et al.* (1997) proposed a modification to equation (2) in order to prevent sag at multiples of $1/T$ (Hz) from appearing in the amplitude spectra. The discretized equation for the modified $F(t)$ is

$$F(t) = \delta(t - t_{ij}) + \frac{1}{n'\left(1 - \frac{1}{e}\right)} \sum_{k=1}^{(N-1)n'} \left[\frac{1}{e^{\frac{(k-1)}{(N-1)n'}}} \delta \left\{ t - t_{ij} - \frac{(k-1)T}{(N-1)n'} \right\} \right]. \quad (4)$$

The shape of equation (4) is shown in Figure 3c. In Irikura (1986), the scaling parameters needed for this technique, N (integer value) and C, can be derived from the constant levels of the displacement and acceleration amplitude spectra of the large and small events with the formulas

$$\frac{U_0}{u_0} = \frac{M_0}{m_0} = CN^3 \quad (5)$$

$$\frac{A_0}{a_0} = CN. \quad (6)$$

Here, U_0 and u_0 indicate the constant levels of amplitude of the displacement spectra for the large and small events, respectively. M_0 and m_0 correspond to the seismic moments for the large and small events. A_0 and a_0 indicate the constant levels of the amplitude of the acceleration spectra for the large and small events (Fig. 3d,e).

N and C are derived from equations (5) and (6):

$$N = \left(\frac{U_0}{u_0}\right)^{1/2} \left(\frac{a_0}{A_0}\right)^{1/2} \quad (7)$$

$$C = \left(\frac{u_0}{U_0}\right)^{1/2} \left(\frac{A_0}{a_0}\right)^{3/2}. \quad (8)$$

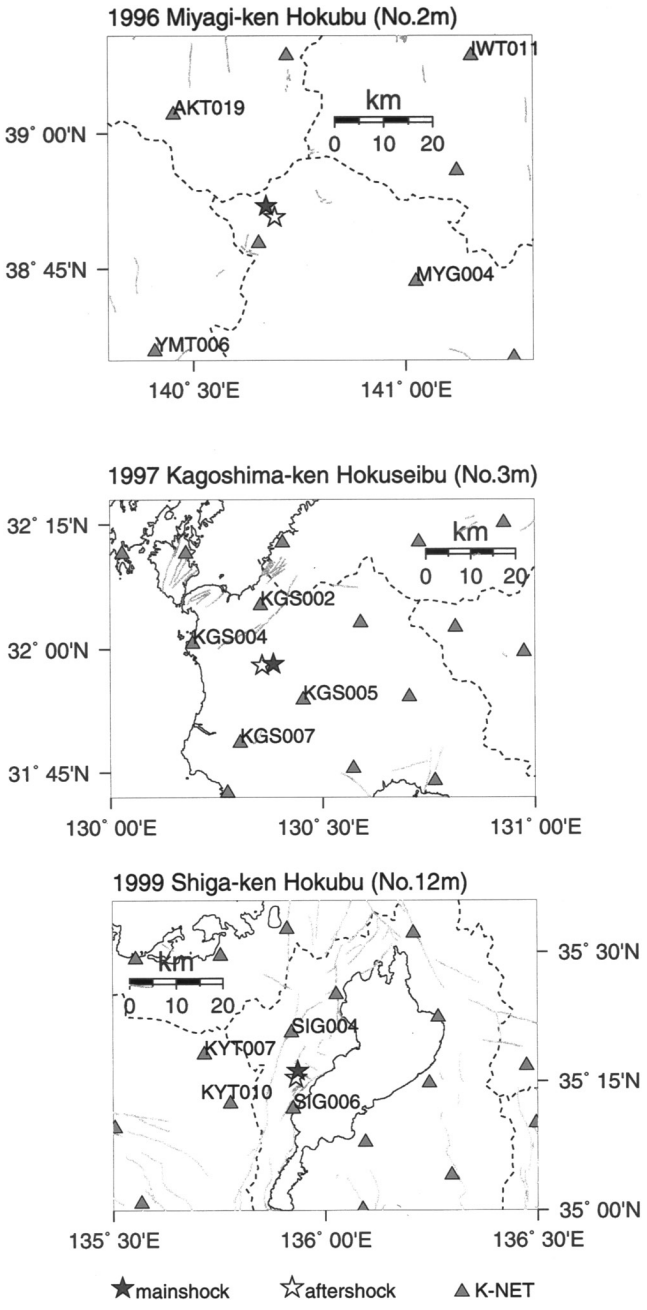

Figure 2. Map showing epicenters of the mainshocks (solid stars) and their foreshocks or aftershocks (open stars) and K-NET stations (triangles) for the earthquakes (numbers 2m, 3m, 12m). Broken lines show the borders between prefectures.

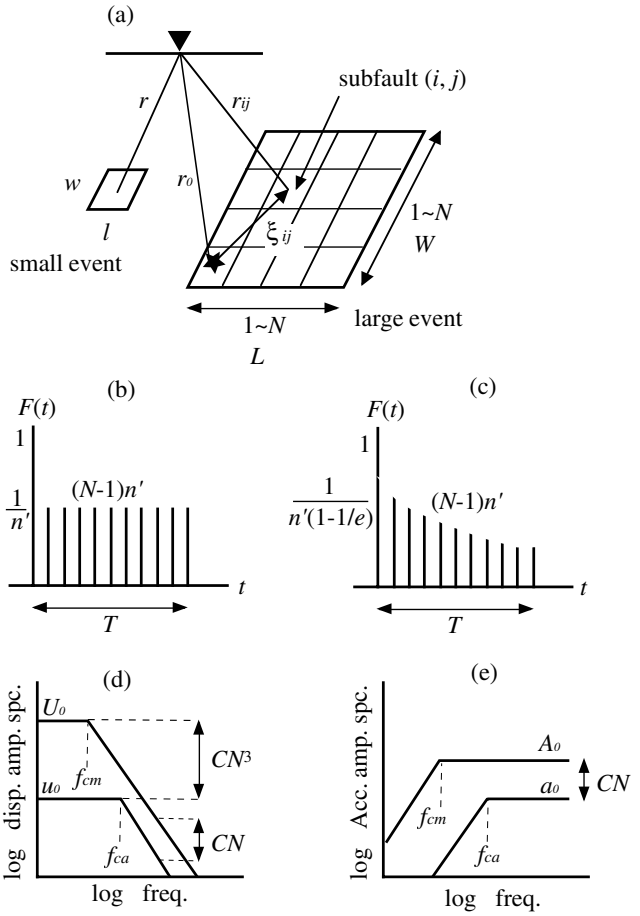

Figure 3. Schematic illustrations of the empirical Green's function method. (a) Fault areas of large and small events are defined to be $L \times W$ and $l \times w$, respectively, where $L/l = W/w = N$. (b) Filtering function $F(t)$ (after Irikura, 1986) to adjust to the difference in slip velocity function between the large and small events. This function is expressed as the sum of a delta and a boxcar function. (c) Modified filtering function (after Irikura *et al.*, 1997) with an exponentially decaying function instead of a boxcar function. T is the rise time for the large event. (d) Schematic displacement amplitude spectra following the omega-squared source scaling model, assuming a stress drop ratio C between the large and small events. (e) Acceleration amplitude spectra following the omega-squared source scaling model.

Parameter Estimation for the Empirical Green's Function Method by the Source Spectral Fitting Method

For an objective estimation of parameters N and C, which are required for the empirical Green's function method of Irikura (1986), Miyake *et al.* (1999) proposed a source spectral fitting method. This method derives these parameters by fitting the observed source spectral ratio between the large and small events to the theoretical source spectral ratio, which obeys the omega-squared source model of Brune (1970, 1971).

The observed waveform $O(t)$ can be expressed as a convolution of the source effect $S(t)$, propagation path effect $P(t)$, and site amplification effect $G(t)$ assuming linear systems:

$$O(t) = S(t)*P(t)*G(t). \quad (9)$$

In the frequency domain, the observed spectrum $O(f)$ is expressed as a product of these effects:

$$O(f) = S(f)\cdot P(f)\cdot G(f). \quad (10)$$

From equation (10), the observed source amplitude spectral ratio of the large and small events for one station is

$$\frac{S(f)}{s(f)} = \frac{O(f)/P(f)}{o(f)/p(f)} = \frac{O(f)\Big/\frac{1}{R}\,e^{-\pi fR/Q_s(f)V_s}}{o(f)\Big/\frac{1}{r}\,e^{-\pi fr/Q_s(f)V_s}}, \quad (11)$$

where capital and lowercase letters indicate factors for large and small events, respectively. The propagation path effect is given by geometrical spreading for the body waves and by a frequency-dependent attenuation factor $Q_s(f)$ for the S waves.

The observed source amplitude spectral ratio for each station is first calculated using the mainshock and its aftershock. Then the observed source amplitude spectral ratio is divided into m windows in the frequency domain, in which the central frequency is f_i ($i = 1$ to m), and the log averages $S(f_i)/s(f_i)$ and the log standard deviations S.D.(f_i) for all stations were obtained (Fig. 4).

The equation for the amplitude spectra, based on the omega-squared source model by Brune (1970, 1971), is given as

$$S(f) = \frac{M_0}{1 + (f/f_c)^2}, \quad (12)$$

where f_c is the corner frequency. Using equation (12), the source spectral ratio function (SSRF) is

$$\mathrm{SSRF}(f) = \frac{M_0}{m_0}\cdot\frac{1 + (f/f_{ca})^2}{1 + (f/f_{cm})^2}. \quad (13)$$

M_0/m_0 indicates the seismic moment ratio between a large and small event at the lowest frequency, and f_{cm} and f_{ca} respectively are corner frequencies for the mainshock and aftershock. We searched the minimum value of the weighted least squares (equation 14), applying to the observed source amplitude spectral ratio, equation (11), to fit the SSRF (equation 13; Fig. 4) in the frequency domain:

$$\sum_{i=1}^{m}\left(\frac{\mathrm{SSRF}\ (f_i) - S(f_i)/s(f_i)}{\mathrm{S.D.}(f_i)}\right)^2 = \min. \quad (14)$$

This method provides estimates of M_0/m_0, f_{cm}, and f_{ca}. The relationships between these parameters, N, and C are given as

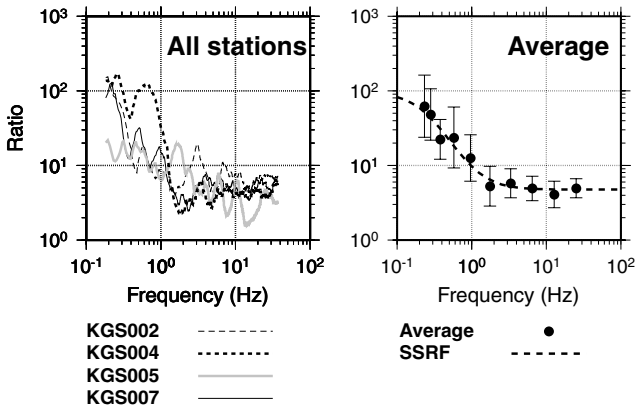

Figure 4. Source spectral ratios of the mainshock to aftershock records used as the empirical Green's function for the 1997 Kagoshima-ken Hokuseibu earthquake, March (number 3m). Left: Spectral ratios for all the sites. Right: Comparison of average values of the observed ratios and best-fit source spectral ratio function (SSRF, broken line). Closed circles represent the average, bars the standard deviation of the observed ratios.

$$\frac{M_0}{m_0} = CN^3 \qquad (f \to 0) \quad (15)$$

$$\left(\frac{M_0}{m_0}\right)\left(\frac{f_{cm}}{f_{ca}}\right)^2 = CN \quad (f \to \infty). \quad (16)$$

The high-frequency limit ($f \to \infty$) corresponds to the frequency where the acceleration source spectrum is constant at frequencies of more than f_{ca} and less than f_{max} (f_{max} is the high-frequency cutoff of the constant level of acceleration source spectrum). According to equations (15) and (16), N and C are

$$N = \frac{f_{ca}}{f_{cm}} \quad (17)$$

$$C = \left(\frac{M_0}{m_0}\right)\left(\frac{f_{cm}}{f_{ca}}\right)^3. \quad (18)$$

Amplitude spectra for 30 sec of the waveforms, including the whole S waves, were calculated by the source spectral fitting method. The vector summation of the three components for the amplitude spectra was used for the analyses. A moving average of $\pm 10\%$ window for each frequency point was applied as a smoothing of amplitude spectra. Parameters for the empirical Green's function method are shown in Table 2, in which the S-wave velocities based on the crustal structure models around the source areas are taken from Hurukawa (1981) and Kakuta *et al.* (1991). The frequency-dependent $Q_s(f)$'s for the S waves were taken from Ogue *et*

Table 2
Source Parameters M_0/m_0, f_{cm}, and f_{ca} Obtained by the Source Spectral Fitting Method (Miyake *et al.*, 1999)

No.	M_0/m_0	f_{cm} (Hz)	f_{ca} (Hz)	N	C	V_s (km)	Range of Analyses (Hz)	K-NET Stations	Name of Earthquake
1m/1a	143.9	0.28	1.31	5	1.41	3.5	0.25–10.0	AKT019, YMT006 MYG004, IWT010	1996 Akita-ken Nairiku Nanbu
2m/2a	10.57	0.63	1.21	2	1.49	3.5	0.20–10.0	AKT019, YMT006 MYG004, IWT011	1996 Miyagi-ken Hokubu
3m/3a	96.2	0.24	1.08	5	1.06	3.1	0.20–10.0	KGS002, KGS004 KGS005, KGS007	1997 Kagoshima-ken Hokuseibu (March)
4m/4a	123.4	0.39	1.43	4	2.50	3.1	0.20–10.0	KGS002, KGS004 KGS005, KGS007	1997 Kagoshima-ken Hokuseibu (May)
5m/5a	416.9	0.20	0.87	4	5.06	3.1	0.30–10.0	YMG001, YMG003 YMG009, SMN014	1997 Yamaguchi-ken Hokubu
6m/6a	16.32	0.72	1.72	2	1.10	3.1	0.40–10.0	TTR007, TTR009 SMN003, SMN015	1997 Tottori-ken Seibu
7m/7a	61.05	0.80	3.60	5	0.67	3.5	0.50–10.0	NIG017, NIG018 NIG020, NIG021	1998 Niigata-ken Chubu
8m/8a	72.69	0.66	2.06	3	2.39	3.5	0.30–10.0	GIF022, SIG008 AIC003, MIE002	1998 Shiga-Gifu Kenkyo
9m/9a	159.9	0.23	1.03	4	1.77	3.5	0.20–10.0	IWT018, IWT021 IWT025, AKT011	1998 Iwate-ken Nairiku Nanbu
10m/10a	74.28	0.72	2.30	3	2.28	3.5	0.20–10.0	MYG012, MYG013 MYG015, YMT010	1998 Miyagi-ken Nanbu
11m/11a	30.21	0.89	2.90	3	0.87	3.5	0.20–10.0	AKT019, AKT020 YMT001, YMT002	1999 Akita-ken Engan Nanbu
12m/12a	238.3	1.12	4.29	4	4.24	3.4	1.00–10.0	SIG004, SIG006 KYT007, KYT010	1999 Shiga-ken Hokubu

N and C are the respective fault size ratios and stress drop ratios of the mainshocks to aftershocks for the empirical Green's function method of Irikura (1986). V_s is the S-wave velocity near the source area.

al. (1997) and Satoh *et al.* (1998). The variations of the spectra at the low frequency are mostly cased by the rupture directivity effects, as shown in the spectral simulation in Miyake *et al.* (2001). They pointed out the importance of having good azimuthal coverage of stations for the determination of source parameters from the spectra, because rupture directivity effects may distort the spectral shapes expected from the omega-square source model and therefore give different corner frequencies and high-frequency decays. The log average values of the observed corner frequencies among several station data were used to weaken the rupture directivity effect.

Near-Source Ground-Motion Simulation to Estimate Strong Motion Generation Area

The modeling of the strong motion generation area using the empirical Green's function method is one of the useful means to kinematically simulate both low- and high-frequency wave generations from the source using the appropriate filtering function $F(t)$. The filtering function $F(t)$ provides the rupture growth with Kostrov-like slip velocity time functions.

Using the source parameters obtained in Table 3, we perform ground-motion simulations of the target earthquakes using the empirical Green's function method in order to estimate the strong motion generation area. These simulations utilized acceleration, velocity, and displacement records from several K-NET stations surrounding the source area. We confirmed that more than four near-source stations are required for source modeling, because there is an azimuthal effect due to rupture directivity (Miyake *et al.*, 2001). The frequency range available for simulation was generally from 0.2 to 10 Hz, depending on the noise levels of the aftershock records. The S-wave arrival times of the velocity waveforms for the target and element earthquakes first were set, then five parameters representing the size (length and width) and position (starting point of the rupture in the strike and dip directions) for the strong motion generation area, and rise time, were estimated to minimize the residuals of the displacement waveform and acceleration envelope fitting. The fitting was done by the genetic algorithm method (e.g., Holland, 1975) for most of the events and by forward modeling for the 1997 Kagoshima-ken Hokuseibu earthquakes (Table 1, numbers 3m and 4m; Miyake *et al.* [1999]). The genetic algorithm method for the parameter determination was operated 10 times for different initial parameters for each source model in order to check the accuracy and stability of the solution. We searched all possibilities for the rupture starting point, and then we did grid searching of length and width of the subfault by 0.1 km and of rise time corresponding to the element earthquake by 0.01 sec. Source modeling is more sensitive for the variation of the rupture starting points rather than the size of the strong motion generation area and rise time (e.g., Miyake *et al.*, 1999). This

Table 3
Parameters for the Strong Motion Generation Area Determined by the Empirical Green's Function Method

No.	SMGA (km^2)	Length (km)	Width (km)	Strike (deg.)	Dip (deg.)	Rise Time (sec)	Starting Point	Name of Earthquake
1m	25.5	8.5	3.0	N358E	47	0.40	(3,5)	1996 Akita-ken Nairiku Nanbu
2m	8.64	3.6	2.4	N225E	84	0.28	(1,2)	1996 Miyagi-ken Hokubu
3m	42.0	7.0	6.0	N278E	89	0.50	(1,5)	1997 Kagoshima-ken Hokuseibu (March)
4m	24.0	3.0 and 3.0	4.0 and 4.0	N280E and N010E	84 and 90	0.50 and 0.50	(1,3) and (1,3)	1997 Kagoshima-ken Hokuseibu (May)
5m	14.4	3.6	4.0	N229E	76	0.28	(2,4)	1997 Yamaguchi-ken Hokubu
6m	5.76	2.4	2.4	N325E	89	0.20	(1,2)	1997 Tottori-ken Seibu
7m	4.00	2.0	2.0	N213E	41	0.10	(1,4)	1998 Niigata-ken Chubu
8m	4.50	3.0	1.5	N024E	67	0.15	(2,3)	1998 Shiga-Gifu Kenkyo
9m	16.0	4.0	4.0	N217E	44	0.32	(1,4)	1998 Iwate-ken Nairiku Nanbu
10m	4.41	2.1	2.1	N203E	37	0.15	(2,3)	1998 Miyagi-ken Nanbu
11m	4.86	2.7	1.8	N181E	66	0.18	(1,3)	1999 Akita-ken Engan Nanbu
12m	1.44	1.2	1.2	N017E or N172E	66 or 26	0.12	(1,3)	1999 Shiga-ken Hokubu

SMGA is the size of the strong motion generation area. Rupture starting points are indicated as (starting fault number of *N* for the strike direction, starting fault number of *N* for the dip direction). Earthquake number 12m has similar residuals for both conjugate fault planes as determined by Fukuyama *et al.* (2000a).

indicates that the rupture directivity effects shown in the waveforms well constrain the rupture starting point in the source modeling. We assumed that rupture propagated radially from the fixed hypocenter at a speed of 90% of the *S*-wave velocity near the source area, except the 1997 Kagoshima-ken Hokuseibu earthquakes.

Following this approach, we estimate the strong motion generation areas for the target earthquakes (M_w 4.8–6.0) (Fig. 1). Synthetic waveforms for the best source models fit the observed data well in acceleration and velocity, while some displacement synthetics seem to be of smaller amplitude than the observations (Fig. 5). The estimated sizes of the strong motion generation areas, rupture starting points in the area, and the rise time are summarized in Table 3. Most of the source models were composed of a single strong motion generation area, except for the 13 May 1997 Kagoshima-ken Hokuseibu earthquake (Table 1, number 4m). We found that this event consisted of two strong motion generation areas, which propagated along both conjugate fault planes. Horikawa (2001) also obtained two asperities, one on each fault plane by kinematic waveform inversion. Rupture propagation directions of the strong motion generation area in the frequency range of 0.2–10 Hz agreed with those of the asperities obtained from low-frequency (<1 Hz) waveform inversion studies, reported by Okada *et al.* (1997) (numbers 1m and 2m), Ide (1999) (number 5m), Nakahara *et al.* (2002) (number 9m), Miyakoshi *et al.* (2000) (numbers 3m, 5m, and 9m), and Horikawa (2001) (numbers 3m and 4m). For the 1999 Shiga-ken Hokubu earthquake (number 12m), estimates of the size of the strong motion generation area and rise time were stable; however, we could not determine the fault plane from the strong ground motion simulation. There was no clear difference in the residuals and shapes of simulated waveforms for the two conjugate fault planes by moment tensor inversion.

Scaling

Relationship between Strong Motion Generation Area and Seismic Moment

For low-frequency source models, the heterogeneous slip distributions of crustal earthquakes have been analyzed to study the characteristics of the slip heterogeneity (e.g., Somerville *et al.*, 1999; Mai and Beroza, 2000, 2002). Somerville *et al.* (1999) studied the slip characterizations by analyzing the heterogeneous slip distributions derived from waveform inversions of strong motion and teleseismic records in the low-frequency range. They found that the size of the asperities (areas of large slip) follows self-similar scaling with respect to seismic moment.

We compare the relationship between the size of the strong motion generation area (0.2–10 Hz) and seismic moment with the scaling relationship characterizing slip distributions of crustal earthquakes (<1 Hz) proposed by Somerville *et al.* (1999) in Figure 6. The strong motion generation area is proportional to $M_0^{2/3}$, indicating self-similar scaling for the range of seismic moments between 1.83×10^{16} N m (M_w 4.8) and 1.38×10^{18} N m (M_w 6.0). As the absolute seismic moment values cannot be estimated from this procedure with the empirical Green's function itself, the seismic moments for the mainshocks are adopted as values determined by moment tensor inversions in Table 1. This scaling of the strong motion generation area is close to that of the combined area of asperities reported by Somerville *et al.* (1999). The effective source area generating strong ground motions occupies almost a quarter of the total rupture area obtained by low-frequency waveform inversions. There is no clear dependence of this scaling depending on rupture propagation direction or focal mechanism. For comparison, we added the combined size of the three strong motion generation areas for the 1994 Northridge earthquake

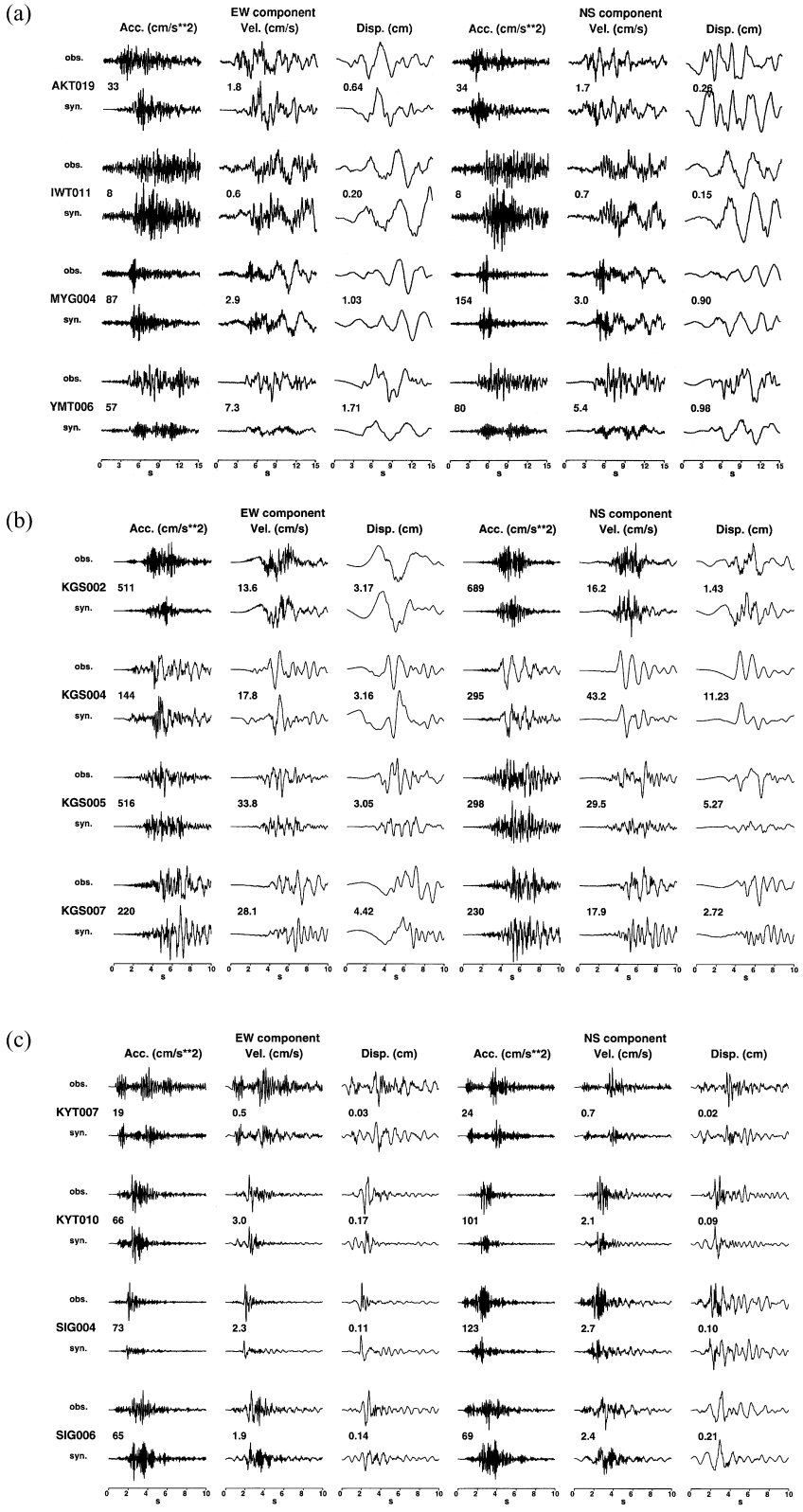

Figure 5. Comparison of observed and synthetic waveforms of acceleration, velocity, and displacement for the (a) 1996 Miyagi-ken Hokubu earthquake (number 2m), (b) 1997 Kagoshima-ken Hokuseibu earthquake, March (number 3m), and (c) 1999 Shiga-ken Hokubu earthquake (number 12m), at the four nearest K-NET stations. Numbers show the maximum amplitude values of the observed waveforms.

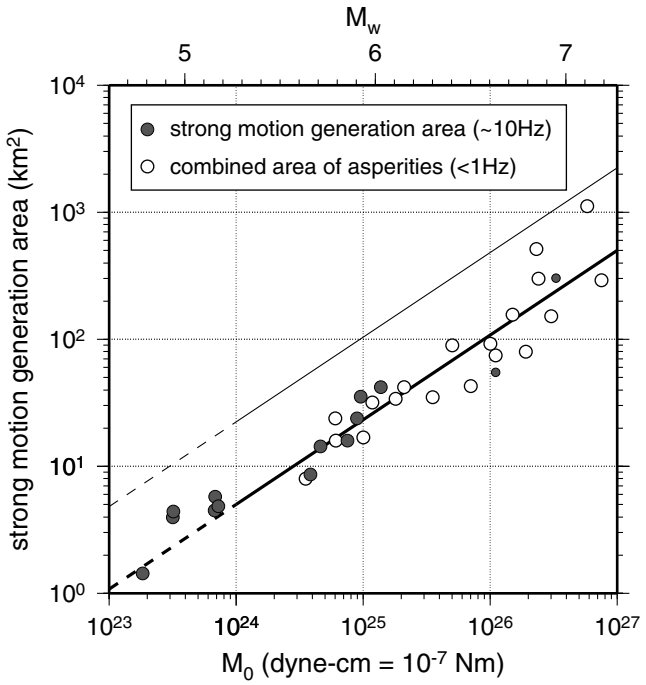

Figure 6. Scaling of the strong motion generation area to seismic moment. Solid and open circles, respectively, show the strong motion generation areas studied and the combined areas of asperities reported by Somerville *et al.* (1999). Thick and thin solid lines respectively correspond to the combined area of asperities and total rupture areas, as a function of the seismic moment (Somerville *et al.*, 1999). Small solid circles are the areas for the 1994 Nothridge earthquake (Kamae and Irikura, 1998b) and for the 1995 Hyogo-ken Nanbu earthquake (Kamae and Irikura, 1998a). The moment magnitude M_w is calculated according to Kanamori (1977).

(M_w 6.6) (Kamae and Irikura, 1998b) and the 1995 Hyogo-ken Nanbu earthquake (M_w 6.8) (Kamae and Irikura, 1998a). They estimated the strong motion generation areas that best fit the velocity and acceleration waveforms by forward modeling. The sizes of their strong motion generation areas are also close to that of the combined area of asperities in Somerville *et al.* (1999).

For several earthquakes, the strong motion generation areas are located at almost the same positions as the asperity areas, based on the criteria of Somerville *et al.* (1999). These asperity areas are determined from the heterogeneous slip distribution results of waveform inversions in the frequency range of 0.1–0.5 Hz (Miyakoshi *et al.*, 2000) (Fig. 7). Our analyses indicate that the large slip areas (asperities from low-frequency waveform inversion) and large slip velocity areas (strong motion generation areas in this study) occupy almost the same regions.

Relationship between Rise Time and Seismic Moment

Figure 8 shows the relationship between the rise time for the strong motion generation area and seismic moment, where we define rise time as the duration of the filtering function $F(t)$. The rise time shows self-similar scaling for earthquake moments less than 1.38×10^{18} N m (M_w 6.0). This scaling is also close to the empirical relationship between rise time and seismic moment derived by Somerville *et al.* (1999). For events larger than M_w 6.5, only the rise time for the largest strong motion generation area of the 1994 Northridge earthquake (Kamae and Irikura, 1998b) follows the empirical relation, whereas that for all strong motion generation areas of the 1995 Hyogo-ken Nanbu earthquake (Kamae and Irikura, 1998a) shows half of the value expected by the empirical relation, regardless of the distance from the hypocenter to the strong motion generation area. At this moment we cannot conclude whether the significantly shorter rise times are required as a characteristic feature of the strong motion generation area for larger events.

Discussion

Source Characterization for Broadband Ground-Motion Simulation

Based on this slip characterization from waveform inversions by Somerville *et al.* (1999), Miyakoshi *et al.* (2000) proposed a characterized source model composed of asperities and a background slip area surrounding the asperities, both regions having a constant slip value. This slip-characterized source model is expressed quantitatively both by outer fault parameters, such as seismic moment or total rupture area, and by inner fault parameters, such as asperity size inside the source. So far this source model has been applied only to simulate low-frequency ground motions, because the slip distributions are obtained from waveform inversion with frequencies less than 1 Hz.

For the broadband ground-motion simulation, we propose a characterized source model composed of strong motion generation areas with large slip velocities and a background slip area with a small slip velocity. To show the importance of slip velocities in our source model, we simulate ground motions for the 26 March 1997 Kagoshima-ken Hokuseibu earthquake (number 3m) in the frequency range of 0.2–10 Hz based on the empirical Green's function method, and we compare differences in synthetic waveforms from the strong motion generation area, background slip area, and both the strong motion generation area and background slip area.

As stated previously, Miyakoshi *et al.* (2000) inverted waveforms to obtain the slip distribution for the 26 March 1997 Kagoshima-ken Hokuseibu earthquake (number 3m) and characterized the slip distribution based on the criteria of Somerville *et al.* (1999). The estimated ratio between the size of the asperity and total rupture area is 0.27, and that of the average slip on the asperity to total rupture area is 1.76. This means that 47.5% (0.27×1.76) of the total seismic moment is generated by the asperity and the other 52.5% by the background slip area. The derived ratio between the size

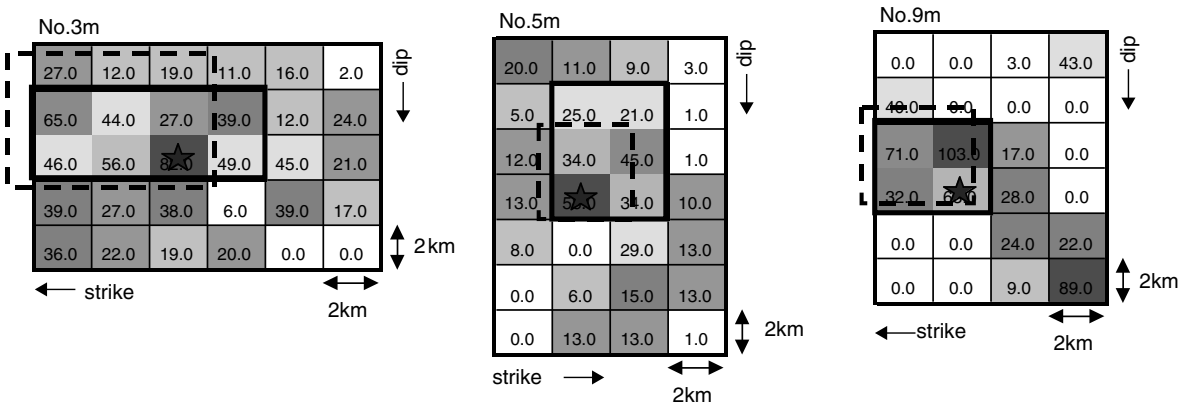

Figure 7. Comparison of the strong motion generation areas and asperity areas, which are characterized from the heterogeneous slip distributions obtained by waveform inversions of Miyakoshi *et al.* (2000). From left to right, the 1997 Kagoshima-ken Hokuseibu earthquake, March (number 3m), 1997 Yamaguchi-ken Hokubu earthquake (number 5m), and 1998 Iwate-ken Nariku Hokubu earthquake (number 9m). Thick solid lines on the total rupture areas show the boundaries of the characterized asperities according to Somerville *et al.* (1999). Broken lines show the boundaries of the strong motion generation areas. Numbers on each subfault are slip, in centimeters, estimated by waveform inversion.

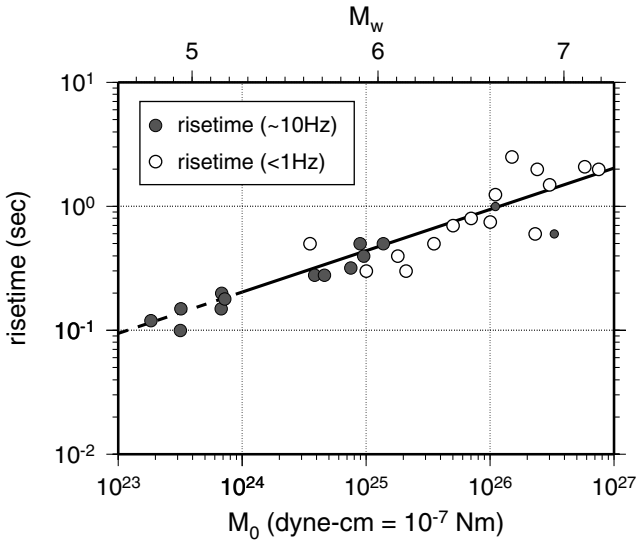

Figure 8. Scaling of the rise time to seismic moment. Solid and open circles, respectively, show the rise times found in this study and which were reported by Somerville *et al.* (1999). Solid line shows the scaling between rise time and seismic moment (Somerville *et al.*, 1999). Small solid circles are the rise times for the 1994 Nothridge earthquake (Kamae and Irikura, 1998b) and for the 1995 Hyogo-ken Nanbu earthquake (Kamae and Irikura, 1998a). The moment magnitude M_w is calculated according to Kanamori (1977).

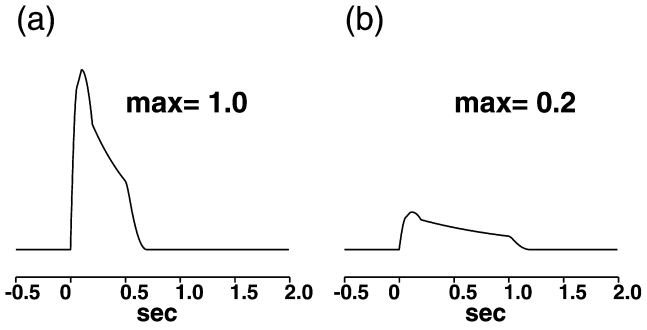

Figure 9. Schematic shape of the synthetic slip velocity time functions on the (a) strong motion generation area and (b) background slip area. The element slip velocity time function is assumed to follow the function proposed by Nakamura and Miyatake (2000). The synthetic slip velocity time functions are expressed as the convolution of the element slip velocity time functions and the filtering functions $F(t)$, given in Figure 3c.

of the background slip area and total rupture area is 0.73 (= 1 − 0.27); therefore the ratio of the average slip on the background slip area to total rupture area is 0.72 (= 0.525/0.73).

We calculate the filtering function, $F(t)$, required in the empirical Green's function method for both the strong motion generation area and background slip area. Aftershock (number 3a) records were adopted as the empirical Green's function. For the strong motion generation area, we used the same $F(t)$ ($N_{\mathrm{SMGA}} = 5$, $C_{\mathrm{SMGA}} = 1.06$, $T_{\mathrm{SMGA}} = 0.5$ sec in Fig. 9a) assuming that our strong motion generation area coincides with the asperity derived by Miyakoshi *et al.* (2000). For the background slip area, we set

$$N_{\mathrm{total}} = \frac{N_{\mathrm{SMGA}}}{\sqrt{\mathrm{SMGA}/S}} = \frac{5}{\sqrt{0.27}} \sim 10, \qquad (19)$$

where S is the size of the total rupture area and SMGA that

of the strong motion generation area. According to Miyakoshi *et al.* (2000), the ratio of seismic moment between the background slip area and strong motion generation area is

$$\frac{M_{0\mathrm{BG}}}{M_{0\mathrm{SMGA}}} = \frac{0.525}{0.475}. \tag{20}$$

This ratio is also expresses as

$$\frac{M_{0\mathrm{BG}}}{M_{0\mathrm{SMGA}}} = \frac{C_{\mathrm{BG}}}{C_{\mathrm{SMGA}}} \cdot \frac{(N_{\mathrm{total}})^2 - (N_{\mathrm{SMGA}})^2}{(N_{\mathrm{SMGA}})^2} \cdot \frac{N_{\mathrm{total}}}{N_{\mathrm{SMGA}}} = \frac{0.20}{1.06} \cdot \frac{10^2 - 5^2}{5^2} \cdot \frac{10}{5}. \tag{21}$$

Because N_{total} is equal to 10 (= twice N_{SMGA}), the duration of $F(t)$ for the background slip area becomes 1.0 sec (= twice T_{SMGA}). The maximum amplitude of $F(t)$ for the background slip area is calculated as about 20% ($C_{\mathrm{BG}} = 0.20$) of that for the strong motion generation area. The $F(t)$ for the background slip area is summarized as $N_{\mathrm{total}} = 10$, $C_{\mathrm{BG}} = 0.20$, and $T_{\mathrm{total}} = 1.0$ sec (Fig. 9b). We calculate the slip velocity time function in each subfault of the target earthquake by convolution between $F(t)$ and the slip velocity time function for a small event. The shape of the slip velocity time function for a small event is schematically calculated by following the formulation of Nakamura and Miyatake (2000). The amplitude of the slip velocity time function for a subfault is larger for the strong motion generation area than for the background slip area, but the duration is shorter (Fig. 10).

The ground motions from the strong motion generation area are almost identical to those from the characterized source model, both in acceleration and velocity (Fig. 10). In contrast, the contribution from the background slip area is small both in acceleration and velocity, although it is slightly more significant in displacement. This suggests that near-source strong ground motions are mainly controlled by the size of the strong motion generation area and its rise time.

Our characterized source model is constructed from the viewpoint of slip velocity, and the target frequency is 0.2–10 Hz. Miyakoshi *et al.* (2000) characterized the heterogeneous source model from the viewpoint of slip itself, and the target frequency is 0.1–0.5 Hz. We showed that the characterized source model of slip at low frequency is equivalent to the characterized source model of slip velocity in the broadband frequency.

Physical Interpretation of the Strong Motion Generation Area

We showed that the strong motion generation area coincides with the asperity area of heterogeneous slip distribution derived from low-frequency (<1 Hz) ground-motion data. We now compare the strong motion generation area with the single-crack and single-asperity model proposed by Das and Kostrov (1986).

Das and Kostrov (1986) discussed the difference between the source amplitude spectrum for the single-asperity model (Fig. 11a) and that for the single-crack model (Fig. 11b), when the size of the asperity and crack are assumed to be the same. They showed that the levels of the source amplitude spectra at high frequencies were almost equal for both models, although at low frequencies they differed by $(R/r)^2$ times due to the slip existence on the stress-free field.

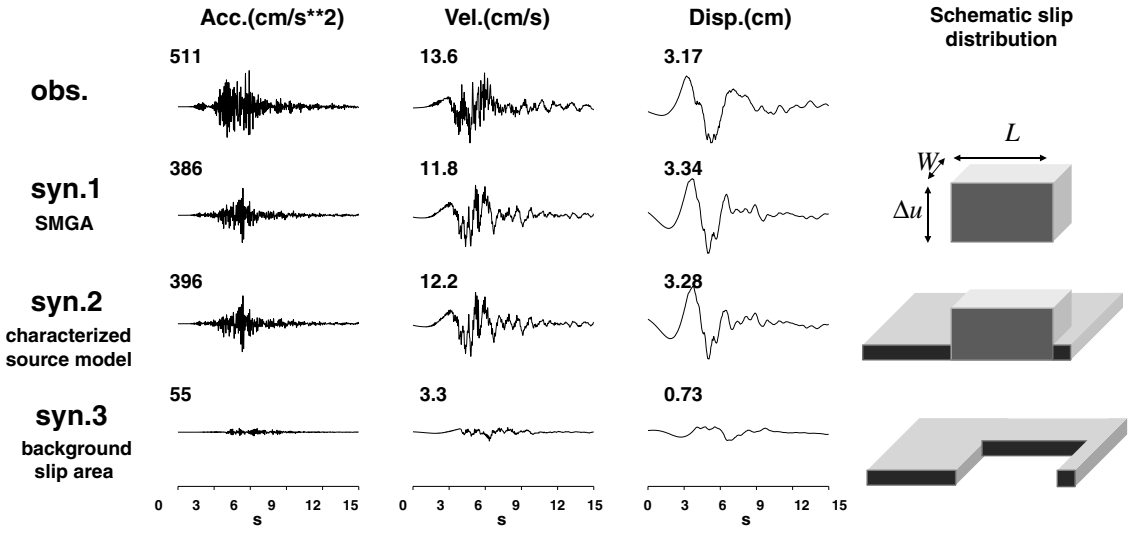

Figure 10. Comparison of observed and synthetic waveforms (0.2–10 Hz) of the east–west component at station KGS002 for the 1997 Kagoshima-ken Hokuseibu earthquake, March (number 3m). Top to bottom: Traces show observed waveforms and synthetic waveforms from the strong motion generation area, both of the strong motion generation area and background slip area in our characterized source model, and background slip area. Left to right: Acceleration, velocity, and displacement waveforms. Numbers above the waveforms are maximum amplitude values.

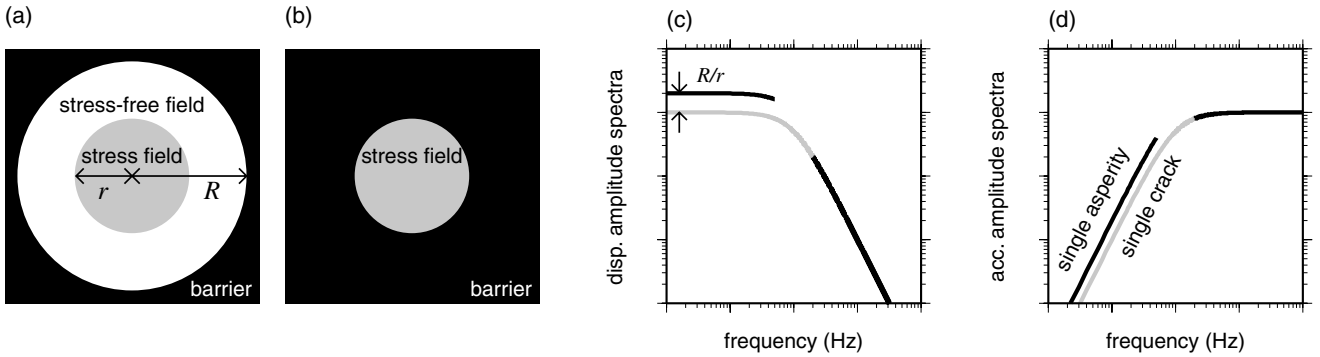

Figure 11. Geometry of (a) single-asperity and (b) single-crack models (after Das and Kostrov 1986). Gray, white, and black zones indicate stress field, stress-free field, and barrier, respectively. (c) Far-field displacement amplitude spectra for the single-asperity (black line) and single-crack (gray line) models at a given magnitude. (d) Far-field acceleration amplitude spectra for the single-asperity (black line) and single-crack (gray line) models at a given magnitude.

We already showed that the ground motions from the strong motion generation area are almost the same as those from the characterized source model both in acceleration and velocity, while they differ in displacement (Fig. 11), indicating that the source models expressed as strong motion generation areas and the characterized source models correspond to the crack and asperity models, respectively. The strong motion generation areas can be regarded as the asperity in the stress-free field.

Stress drop for the strong motion generation area is calculated based on the formulation of Madariaga (1979) and Boatwright (1988), assuming the single-asperity model. The background slip area is assumed to have no stress drop. The equation for the stress drop in the strong motion generation area, $\Delta\sigma_{\mathrm{SMGA}}$, is

$$\Delta\sigma_{\mathrm{SMGA}} = \frac{7}{16} \cdot \frac{M_0}{Rr^2}, \tag{22}$$

where M_0 is the seismic moment for the target earthquake, R the equivalent radius for the total rupture area S ($S = \pi R^2$), and r the equivalent radius for the strong motion generation area SMGA (SMGA $= \pi r^2$). Note that the displacement amplitude spectrum of the single asperity is (R/r) times of that of the single-crack models (Fig. 11c), while Das and Kostrov (1986) pointed out $(R/r)^2$ times difference. This difference occurs because Madariaga (1979) and Boatwright (1988) used the average slip of the crack in the reciprocal theorem to derive equation (22) assuming the asperity located at an arbitrary position of the stress-free field, while Das and Kostrov (1986) used the maximum slip of the crack assuming a small asperity at the center of the stress-free field.

The stress drops in the strong motion generation areas for crustal earthquakes were calculated using equation (21), where we used the total rupture areas S (in Fig. 7) estimated by Miyakoshi *et al.* (2000). The values of the stress drop are estimated to be about 10 MPa (Table 4).

Table 4
Total Rupture Area, Strong Motion Generation Area, and Estimated Stress Drop in the Strong Motion Generation Area

No.	S (km^2)	SMGA (km^2)	$\Delta\sigma_{SMGA}$ (MPa)	Name of Earthquake
3m	120	42.0	7.29	1997 Kagoshima-ken Hokuseibu (March)
5m	112	14.4	7.35	1997 Yamaguchi-ken Hokubu
9m	100	16.0	11.46	1998 Iwate-ken Nairiku Nanbu

The total rupture areas are those Miyakoshi *et al.* (2000) estimated by waveform inversion.

Conclusions

We show that the strong motion generation areas obtained in this study (0.2–10 Hz) coincide with the areas of the asperities of heterogeneous slip distributions derived from low-frequency (<1 Hz) waveform inversions. The self-similar scalings for the size of the strong motion generation area and rise time, as a function of seismic moment, are found for the range of earthquakes less than M_{w} 6.0. These scalings are compatible with those for larger earthquakes obtained by Somerville *et al.* (1999).

Our analyses suggest that source characterization for simulating the broadband frequency ground motion requires strong motion generation areas that produce high-frequency motions with large slip velocities as well as a background slip area that produces low-frequency motions with a small slip velocity. The near-source strong ground motions are controlled mainly by the size of the strong motion generation area and rise time there. The characterized source model presented in this study looks different from the high-frequency source models from envelope inversions; however, we address the fact that strong motion generation areas with 10 MPa stress drop can also reproduce a series of high-frequency waveforms.

The strong motion generation area contains both low- and high-frequency information that is scaled to the wave generations and rupture dynamics of small earthquakes. We verified that quantified strong motion generation areas and the idea of the characterized source modeling have enough ability to perform the broadband ground-motion simulation in acceleration, velocity, and displacement.

Acknowledgments

We are greatly indebted to K-NET for the strong ground motion data. We would like to thank Keiko Kuge, Harvard CMT catalog, and NIED seismic moment tensor catalog for the focal mechanism information and the Faculty of Science, Kyushu University and JMA, who provided the hypocenter information. We are also grateful to Ken Miyakoshi for giving us the results of the waveform inversion, Jorge Aguirre for his helpful support in the use of the genetic algorithm, and Jim Mori for improvement of this manuscript. We are very grateful to Mariagiovanna Guatteri and Martin Mai for reviewing the manuscript and providing valuable comments. Some figures were drawn by GMT Ver.3.0 (Wessel and Smith, 1995). H.M. was supported by Research Fellowships for Young Scientists from the Japan Society for the Promotion of Science. This work was supported in part by a Grant-in-Aid for Scientific Research (Number 11209201) and the Special Coordination Funds titled "Study on the master model for strong ground motion prediction toward earthquake disaster mitigation" from the Ministry of Education, Science, Sports, and Culture of Japan.

References

Aki, K. (1967). Scaling law of seismic spectrum, *J. Geophys. Res.* **72,** 1217–1231.

Beroza, G. C. (1991). Near-source modeling of the Loma Prieta earthquake: evidence for heterogeneous slip and implications for earthquake hazard, *Bull. Seism. Soc. Am.* **81,** 1603–1621.

Boatwright, J. (1988). The seismic radiation from composite models of faulting, *Bull. Seism. Soc. Am.* **78,** 489–508.

Bouchon, M., M. N. Toksöz, H. Karabulut, and M. -P. Bouin (2002). Space and time evolution of rupture and faulting during the 1999 İzmit (Turkey) earthquake, *Bull. Seism. Soc. Am.* **92,** 256–266.

Brune, J. N. (1970). Tectonic stress and the spectra of seismic shear waves from earthquakes, *J. Geophys. Res.* **75,** 4997–5009.

Brune, J. N. (1971). Correction, *J. Geophys. Res.* **76,** 5002.

Chi, W. C., D. Dreger, and A. Kaverina (2001). Finite-source modeling of the 1999 Taiwan (Chi-Chi) earthquake derived from a dense strong-motion network, *Bull. Seism. Soc. Am.* **91,** 1144–1157.

Cohee, B. P., and G. C. Beroza (1994). Slip distribution of the 1992 Landers earthquake and its implications for earthquake source mechanics, *Bull. Seism. Soc. Am.* **84,** 692–172.

Cotton, F., and M. Campillo (1995). Frequency domain inversion of strong motions: application to the 1992 Landers earthquake, *J. Geophys. Res.* **100,** 3961–3975.

Das, S., and B. V. Kostrov (1986). Fracture of a single asperity on a finite fault: a model for weak earthquakes? in *Earthquake Source Mechanics*, S. Das, J. Boatwright, and C. H. Scholz (Editors), American Geophysical Monograph 37, 91–96.

Delouis, B., D. Giardini, P. Lundgren, and J. Salichon (2002). Joint inversion of InSAR, GPS, teleseismic, and strong-motion data for the spatial and temporal distribution of earthquake slip: application to the 1999 İzmit mainshock, *Bull. Seism. Soc. Am.* **92,** 278–299.

Dziewonski, A. M., G. Ekstrom, and M. P. Salganik (1996). Centroid-moment tensor solutions for January–March 1995, *Phys. Earth Planet. Interiors* **93,** 147–157.

Dziewonski, A. M., G. Ekstrom, N. N. Maternovskaya, and M. P. Salganik (1997). Centroid-moment tensor solutions for July–September 1996, *Phys. Earth Planet. Interiors* **102,** 133–143.

Faculty of Science, Kagoshima University (1997). The earthquakes with *M* 6.3 (March 26, 1997) and with *M* 6.2 (May 13, 1997) occurring in northwestern Kagoshima prefecture, Rep. Coord. Comm. Earthquake Pred. 58, 630–637 (in Japanese).

Faculty of Science, Kyushu University (1997). Seismic activity in Kyushu (November 1996–April 1997), Rep. Coord. Comm. Earthquake Pred. 58, 605–618 (in Japanese).

Fukuoka District Meteorological Observatory, JMA (1998). On an *M* 6.3 earthquake in the northern Yamaguchi prefecture on June 25, 1997, Rep. Coord. Comm. Earthquake Pred. 59, 507–510 (in Japanese).

Fukuyama, E., M. Ishida, S. Horiuchi, H. Inoue, S. Hori, S. Sekiguchi, H. Kawai, H. Murakami, S. Yamamoto, K. Nonomura, and A. Goto (2000a). NIED seismic moment tensor catalogue January–December, 1999, Technical Note of the National Research Institute for Earth Science and Disaster Prevention 199, 1–56.

Fukuyama, E., M. Ishida, S. Horiuchi, H. Inoue, S. Hori, S. Sekiguchi, A. Kubo, H. Kawai, H. Murakami, and K. Nonomura (2000b). NIED seismic moment tensor catalogue January–December, 1997, Technical Note of the National Research Institute for Earth Science and Disaster Prevention 205, 1–35.

Fukuyama, E., M. Ishida, S. Horiuchi, H. Inoue, A. Kubo, H. Kawai, H. Murakami, and K. Nonomura (2001). NIED seismic moment tensor catalogue January–December, 1998 (revised), Technical Note of the National Research Institute for Earth Science and Disaster Prevention 218, 1–51.

Graduate School of Science, Tohoku University (1999). On the seismic activity of the *M* 6.1 earthquake of 3 September 1998 in Shizukuishi, Iwate prefecture, Rep. Coord. Comm. Earthq. Pred. 60, 49–53 (in Japanese).

Hartzell, S. H. (1978). Earthquake aftershocks as Green's functions, *Geophys. Res. Lett.* **5,** 1–4.

Harzell, S. H., and T. H. Heaton (1983). Inversion of strong ground motion and teleseismic waveform data for the fault rupture history of the 1979 Imperial Valley, California, earthquake, *Bull. Seism. Soc. Am.* **73,** 1553–1583.

Holland, J. H. (1975). *Adaptation in Natural and Artificial Systems*, University of Michigan Press, Ann Arbor.

Horikawa, H. (2001). Earthquake doublet in Kagoshima, Japan: rupture of asperities in a stress shadow, *Bull. Seism. Soc. Am.* **91,** 112–127.

Horikawa, H., K. Hirahara, Y. Umeda, M. Hashimoto, and F. Kusano (1996). Simultaneous inversion of geodetic and strong motion data for the source process of the Hyogo-ken Nanbu, Japan, earthquake, *J. Phys. Earth* **44,** 455–471.

Hurukawa, N. (1981). Normal faulting microearthquakes occurring near the moho discontinuity in the northeastern Kinki district, Japan, *J. Phys. Earth* **29,** 519–535.

Ide, S., M. Takeo, and Y. Yoshida (1996). Source process of the 1995 Kobe earthquake: determination of spatiotemporal slip distribution by Bayesian modeling, *Bull. Seism. Soc. Am.* **86,** 547–566.

Ide, S. (1999). Source process of the 1997 Yamaguchi, Japan, earthquake analyzed in different frequency bands, *Geophys. Res. Lett.* **26,** 1973–1976.

Irikura, K. (1983). Semi-empirical estimation of strong ground motions during large earthquakes, *Bull. Disast. Prev. Res. Inst. Kyoto Univ.* **33,** 63–104.

Irikura, K. (1986). Prediction of strong acceleration motions using empirical Green's function, in *Proc. 7th Japan Earthquake Engineering Symp.*, 151–156, Tokyo, 10–12 December 1986.

Irikura, K., and K. Kamae (1994). Estimation of strong ground motion in broad-frequency band based on a seismic source scaling model and an empirical Green's function technique, *Ann. Geofis.* **37,** 1721–1743.

Irikura, K., T. Kagawa, and H. Sekiguchi (1997). Revision of the empirical Green's function method by Irikura (1986) (program and abstracts), *Seism. Soc. Japan* **2,** B25 (in Japanese).

Kakehi, Y., and K. Irikura (1996). Estimation of high-frequency wave radiation areas on the fault plane by the envelope inversion of acceleration seismograms, *Geophys. J. Int.* **125,** 892–900.

Kakuta, T., H. Miyamachi, and A. Takagi (1991). Intermediate earthquakes

in a northern part of the Kyushu–Ryukyu arc, *Zisin* **44,** 63–74 (in Japanese with English abstract).

Kamae, K., and K. Irikura (1998a). Source model of the 1995 Hyogo-ken Nanbu earthquake and simulation of near-source ground motion, *Bull. Seism. Soc. Am.* **88,** 400–412.

Kamae, K., and K. Irikura (1998b). A source model of the 1994 Northridge earthquake (M_w 6.7), in *Proc. 10th Japan Earthquake Engineering Symp.*, 643–648, Yokohama, Japan, 25–27 November 1998 (in Japanese with English abstract).

Kanamori, H. (1977). The energy release in great earthquakes, *J. Geophys. Res.* **82,** 2981–2987.

Kanamori, H. (1979). A semi-empirical approach to prediction of long-period ground motions from great earthquakes, *Bull. Seism. Soc. Am.* **69,** 1645–1670.

Kanamori, H., and D. L. Anderson (1975). Theoretical basis of some empirical relations in seismology, *Bull. Seism. Soc. Am.* **65,** 1073–1095.

Kawase, H. (1998). Metamorphosis of near-field strong motions by underground structures and their destructiveness to man-made structures, learned from the damage belt formation during the Hyogo-ken Nanbu earthquake of 1995, in *Proc. 10th Japan Earthquake Engineering Symp.*, 29–34, Yokohama, Japan, 25–27 November 1998 (in Japanese with English abstract).

Kinoshita, S. (1998). Kyoshin Net (K-NET), *Seism. Res. Lett.* **69,** 309–332.

Kuge, K. (2003). Source modeling using strong-motion waveforms: toward automated determination of earthquake fault planes and moment-release distributions, *Bull. Seism. Soc. Am.* **93,** 639–654.

Kuge, K., T. Iwata, and K. Irikura (1997). Automatic estimation of earthquake source parameters using waveform data from the K-NET (programme and abstracts), *Seism. Soc. Japan* **2,** B16 (in Japanese).

Ma, K. F., J. Mori, S. J. Lee, and S. B. Yu (2001). Spatial and temporal distribution of slip for the 1999 Chi-Chi, Taiwan, earthquake, *Bull. Seism. Soc. Am.* **91,** 1069–1087.

Madariaga, R. (1979). On the relation between seismic moment and stress drop in the presence of stress and strength heterogeneity, *J. Geophys. Res.* **84,** 2243–2250.

Mai, P. M., and G. C. Beroza (2000). Source scaling properties from finite-fault rupture models, *Bull. Seism. Soc. Am.* **90,** 604–615.

Mai, P. M., and G. C. Beroza (2002). A spatial random-field model to characterize complexity in earthquake slip, *J. Geophys. Res.* **107,** no. B11, 2308, doi 10.1029/2001JB000588.

Miyake, H., T. Iwata, and K. Irikura (1999). Strong ground motion simulation and source modeling of the Kagoshima-ken Hokuseibu earthquakes of March 26 (M_{JMA} 6.5) and May 13 (M_{JMA} 6.3), 1997, using empirical Green's function method, *Zisin* **51,** 431–442 (in Japanese with English abstract).

Miyake, H., T. Iwata, and K. Irikura (2001). Estimation of rupture propagation direction and strong motion generation area from azimuth and distance dependence of source amplitude spectra, *Geophys. Res. Lett.* **28,** 2727–2730.

Miyakoshi, K., T. Kagawa, H. Sekiguchi, T. Iwata, and K. Irikura (2000). Source characterization of inland earthquakes in Japan using source inversion results, in *Proc. 12th World Conf. Earthquake Engineering*, Aukland, New Zealand, 30 January–4 February (CD-ROM).

Miyamachi, H., K. Iwakiri, H. Yakiwara, K. Goto, and T. Kakuta (1999). Fine structure of aftershock distribution of the 1997 northwestern Kagoshima earthquakes with a three-dimensional velocity model, *Earth Planet Space* **51,** 233–246.

Nakamura, H., and T. Miyatake (2000). An approximate expression of slip velocity time function for simulation of near-field strong ground motion, *Zisin* **53,** 1–9 (in Japanese with English abstract).

Nakahara, H., T. Nishimura, H. Sato, and M. Ohtake (1998). Seismogram envelope inversion for the spatial distribution of high-frequency energy radiation from the earthquake fault: application to the 1994 far east off Sanriku earthquake, Japan, *J. Geophys. Res.* **103,** 855–867.

Nakahara, H., T. Nishimura, H. Sato, M. Ohtake, S. Kinoshita, and H. Hamaguchi (2002). Broadband source process of the 1998 Iwate prefecture, Japan, earthquake as revealed from inversions analyses of seismic waveforms and envelopes, *Bull. Seism. Soc. Am.* **92,** 1708–1720.

Ogue, Y., Y. Wada, A. Narita, and S. Kinoshita (1997). Deconvolution for the K-NET data from earthquake in southern Kyushu (program and abstracts), *Seism. Soc. Japan* **2,** B23 (in Japanese).

Okada, T., N: Umino, A. Hasegawa, and N. Nishide (1997). Source processes of the earthquakes in the border of Akita and Miyagi prefectures in August, 1996 (2) (program and abstracts), *Seism. Soc. Japan* **2,** B69 (in Japanese).

Satoh, T., H. Kawase, and S. Matsushima (1998). Source spectra, attenuation function, and site amplification factors estimated from the K-NET records for the earthquakes in the border of Akita and Miyagi prefectures in August, 1996, *Zisin* **50,** 415–429 (in Japanese with English abstract).

Sekiguchi, H., and T. Iwata (2002). Rupture process of the 1999 Kocaeli, Turkey, earthquake estimated from strong-motion waveforms, *Bull. Seism. Soc. Am.* **92,** 300–311.

Sekiguchi, H., K. Irikura, and T. Iwata (2000). Fault geometry at the rupture termination of the 1995 Hyogo-ken Nanbu Earthquake, *Bull. Seism. Soc. Am.* **90,** 117–133.

Sekiguchi, H., K. Irikura, T. Iwata, Y. Kakehi, and M. Hoshiba (1996). Minute locating of faulting beneath Kobe and the waveform inversion of the source process during the 1995 Hyogo-ken Nanbu, Japan, earthquake using strong ground motion records, *J. Phys. Earth* **44,** 473–487.

Somerville, P., K. Irikura, R. Graves, S. Sawada, D. Wald, N. Abrahamson, Y. Iwasaki, T. Kagawa, N. Smith, and A. Kowada (1999). Characterizing crustal earthquake slip models for the prediction of strong ground motion, *Seism. Res. Lett.* **70,** 59–80.

Umino, N., T. Matsuzawa, S. Hori, A. Nakamura, A. Yamamoto, A. Hasegawa, and T. Yoshida (1998). 1996 Onikobe earthquakes and their relation to crustal structure, *Zisin* **51,** 253–264 (in Japanese with English abstract).

Wald, D. J. (1996). Slip history of the 1995 Kobe, Japan, earthquake determined from strong motion, teleseismic, and geodetic data, *J. Phys. Earth* **44,** 489–503.

Wald, D. J., and T. H. Heaton (1994). Spatial and temporal distribution of slip of the 1992 Landers, California, earthquake, *Bull. Seism. Soc. Am.* **84,** 668–691.

Wald, D. J., T. H. Heaton, and K. W. Hudnut (1996). The slip history of the 1994 Northridge, California, earthquake determined from strong-motion, teleseismic, GPS, and leveling data, *Bull. Seism. Soc. Am.* **86,** S49–S70.

Wald, D. J., D. V. Helmberger, and T. H. Heaton (1991). Rupture model of the 1989 Loma Prieta earthquake from the inversion of strong motion and broadband teleseismic data, *Bull. Seism. Soc. Am.* **81,** 1540–1572.

Wessel, P., and W. H. F. Smith (1995). New version of the Generic Mapping Tools released, *EOS* **76,** 329.

Wu, C., M. Takeo, and S. Ide (2001). Source process of the Chi-Chi earthquake: a joint inversion of strong motion data and global positioning system data with a multifault model, *Bull. Seism. Soc. Am.* **91,** 1028–1043.

Yoshida, S., K. Koketsu, B. Shibazaki, T. Sagiya, T. Kato, and Y. Yoshida (1996). Joint inversion of near- and far-field waveforms and geodetic data for the rupture process of the 1995 Kobe earthquake, *J. Phys. Earth* **44,** 437–454.

Zeng, Y., and C. H. Chen (2001) Fault rupture process of the 20 September 1999 Chi-Chi, Taiwan, earthquake, *Bull. Seism. Soc. Am.* **91,** 1088–1098.

Zeng, Y., K. Aki, and T. Teng (1993). Mapping of the high-frequency source radiation for the Loma Prieta earthquake, California, *J. Geophys. Res.* **98,** 11,981–11,993.

Disaster Prevention Research Institute
Kyoto University
Gokasho, Uji, Kyoto 611-0011, Japan
miyake@egmdpri01.dpri.kyoto-u.ac.jp

Manuscript received 22 August 2002.